Contents lists available at Science-Gate

International Journal of Advanced and Applied Sciences

Journal homepage: http://www.science-gate.com/IJAAS.html

Influence of variable thermal conductivity on axisymmetric slip flow in a pipe with a varying radius

Mohamed H. Hendy [1,*], Abaker A. Hassaballa [2], Mnahil M. Bashier [2]

[1]Department of General Courses, Applied College, Northern Border University, Arar, Saudi Arabia
[2]Department of Mathematics, Faculty of Science, Northern Border University, Arar, Saudi Arabia

ARTICLE INFO

Article history:
Received 2 October 2024
Received in revised form
25 January 2025
Accepted 25 April 2025

Keywords:
Wave propagation
Elastic orthotropic tubes
Slip velocity
Low Reynolds number flow
Pressure drop analysis

ABSTRACT

This study examines wave propagation in elastic orthotropic tubes filled with a uniformly tapered fluid, focusing on the effects of slip velocity variations at the tube wall. A Newtonian fluid flows through tubes with different radii, and microscale gas flows may be influenced by temperature gradients, affecting viscosity and temperature-dependent thermal conductivity. An asymptotic series solution for low Reynolds number flow is employed to determine streamlines, velocity profiles, and variations in amplitude and wavelength of constrictions. A closed-form formula is derived to calculate the pressure drop, improving upon the Hagen-Poiseuille model by accounting for wavelength effects. Axisymmetric solutions to the governing differential equations are obtained under the assumption of no traction on the outer wall surface. Numerical analysis reveals that the slip parameter significantly influences axial and radial velocities as well as temperature profiles, providing insights into fluid behavior in elastic tubes.

© 2025 The Authors. Published by IASE. This is an open access article under the CC BY-NC-ND license (http://creativecommons.org/licenses/by-nc-nd/4.0/).

1. Introduction

Intravascular plaques frequently cause stenosis, a localized constriction of an artery in humans or animals. This narrowing of the artery prevents blood from flowing normally. Serious problems, such as tissue growth in the artery, coronary thrombosis, and arterial weakening and bulging downstream from the stenosis, may be better understood by gaining a better grasp of the flow patterns close to the stenosis. Whole blood pulsating through a cylinder is the subject of research (El-Khatib et al., 2003). For further information on pulsatile blood flow analysis in a model bifurcated artery with stenosis in the parent arterial lumen, refer to Chakravarty (2008) and Panlogism et al. (2017). Srinivasacharya and Rao's (2016) investigations on wave propagation in fluid-filled tubes have been ongoing for quite some time, but many important details remain unsolved. The tubes were thought to be connected. Using the resulting analytical formulas and adequate data for the parameters involved, numerical estimates of numerous variables of physical importance have been attempted for a particular instance of blood flow via a tapering artery section, which is in tethered condition. Teimouri et al. (2021) studied the effect of an external magnetic field on the shape of plaque as a function of fluctuations in pulsatile blood flow in a stenosed curved artery. Arteriosclerotic blood vessels and pipe flow may be better understood by studying flows in tubes of varied radii. Both steady-state and pulse-wave blood flow were used to test the carotid artery's stability (Khalafvand et al., 2015).

Manton (1971) examined the concept of constant flow in a tube with a radius that varied slowly. Chow and Soda (1972) investigated the steady-state flow in a tube with a roughness wall of arbitrarily high spread relative to the tube's mean radius. This method presupposes, without explicitly saying so, that even when the radius is a periodic function of the axial variable, all disturbances to the velocity are zero at infinity. By increasing the stream function by powers of the ostensibly small ratio between the orders of magnitude of average oscillatory and stable axial velocities, Rao and Devanathan (1973) examined slow pulsatile flow in tubes with slowly varying cross sections. The gradual change in the cross-section of a tube carrying a viscous fluid is a basic idea having physiological and technical implications.

Ponalagusamy and Priyadharshini (2017) studied the nonlinear model of pulsatile flow of blood

* Corresponding Author.
Email Address: hendy442003@yahoo.com (M. H. Hendy)
https://doi.org/10.21833/ijaas.2025.04.020
Corresponding author's ORCID profile:
https://orcid.org/0000-0003-1919-1647
2313-626X/© 2025 The Authors. Published by IASE.
This is an open access article under the CC BY-NC-ND license (http://creativecommons.org/licenses/by-nc-nd/4.0/)

through a porous bifurcated arterial stenosis. When seen through a physiological lens, blood flows through the body's main arteries as a viscous fluid according to Newton's laws of motion (Shankar et al., 2019). Newtonian fluid pressure wave propagation in uniformly convergent and divergent thin-walled orthotropic elastic tubes: a theoretical study. There are axisymmetric solutions to the differential equations that control the fluid and solid elastic wall motions. Flowing in an axisymmetric rotating tube has been the subject of much research in theory and experiment. The presence of stenosis on the arterial walls alters blood flow, which in turn causes vascular diseases. This is a well-known fact in the field of biomechanics. Regarding biomechanics, the development of artificial blood vessels and comprehension of how blood flows in arteries depend on research into blood flow in tapered geometries. Although they work better with tubes of uniform diameter, there would be no hemodynamic benefit to employing tapered lumen grafts. The blood flow velocity increases with distance due to the gradual reduction in the cross-sectional area of a tapered lumen. The flow of a Newtonian fluid through an axisymmetrically constricted tube at low Reynolds numbers has several solutions. A simple model may estimate the flow by supposing Hagen-Poiseuille flow at each axial position along the tube. The Hagen-Poiseuille equation is integrated across the tube length to get the total pressure drop. Even though tubes with small constrictions may still provide satisfactory results, this method becomes less accurate as the amplitude of the constriction becomes large; for more, see Sisavath et al. (2001a). Methods such as the geometric iteration method, the collocation method (Tilton and Payatakes, 1984), or the boundary integral method are numerical approaches that may be used to solve the Navier-Stokes equation. The approximate analytical solution for the flow of a Phan-Thien-Tanner fluid through an axisymmetric hyperbolic contraction with slip boundary condition is investigated in Boraey and Guaily (2021) and Pérez-Salas et al. (2021) for the quasi-two-dimensional non-isothermal fully developed flow of molten salt in a circular pipe. Bilal et al. (2022) studied the magneto nanofluid flow over partially slip and convective cylinders with thermal radiation. According to Hemmat et al. (1995), these methods may provide a range of valuable outcomes that are usually in agreement with experimental data, even when the Reynolds number is higher than the one at which flow recirculation begins. White (1962), Terrill and Thomas (1969), and Terrill (1984) were a few examples of works that discuss laminar flow in porous rectangular channels and porous cylindrical pipes, respectively. Applying a perturbation analysis to the Navier-Stokes equation for low Reynolds number, slowly evolving tubes, by Sisavath et al. (2001a). The classical laminar boundary layer equations are solved using the nonlinear Navier boundary condition (Matthews and Hill, 2007; 2008). A fundamental concept of viscous liquid mechanics is the "no-slip" boundary condition. On the other hand, there are several cases when this assumption is wrong seen in Koplik (1982) and Elshahed (2004). A study conducted by Singh (2013) examined the significant effects of sliding against a wall and observed. A thin film of fluid flowing in streams at the boundary area immediately below the permeable surface is connected to the slip velocity, which is inversely related to the shear rate there (Singh and Laurence, 1979). Furthermore, the slip suits specific chemical engineering and other application difficulties (Chu, 2000; Rao and Rajagopal, 1999; Wong, 2002). The validity of the continuum approach relies on the value of the Knudsen number (Kn). This non-dimensional parameter is the fluid molecules' mean free path ratio to the fluid passage's dimensions. This is even though fluid is typically treated as a continuous medium in flow through microdomains. The fluid is seen to lose its hold on borders and slide over the domain walls if Kn is between 0.001 and 0.1 (Vasudeviah et al., 1999). In their study, Fusi et al. (2020); the movement of a Bingham fluid through a conduit with a radius that can be changed. Kakaç et al. (2011) investigated how viscosity and thermal conductivity changes impacted heat transmission in slip flow between single phases.

This work addresses the slow, unsteady flow in an axisymmetric tube of arbitrarily changeable radius, and its objective is to examine the influence of slip velocity on the steady flow of a Newtonian fluid through such a tube. The cross-section of the tube may be varied. An axisymmetric tube with a radius that varies sinusoidally is subjected to the asymptotic solution that was first proposed by Manton (1971) and subsequently revised by Van Dyke (1987). Analyzed numerically is a specific example of flow in a tube with a sinusoidal border. Using analytical and numerical methods, we were able to solve this problem. We anticipate that the paper's findings will be useful in future research on blood flow through individual arterial segments and, more specifically, in studying how small amplitude harmonic waves produced by blood flow propagate through such segments when the wavelength is much larger than their radius.

2. Formulation and analysis

The steady-state Navier-Stokes equations for a Newtonian fluid flowing through an axisymmetric tube with a radius R(z) (Fig. 1) that might change are expressed in terms of the cylindrical coordinate system (r, z) as:

$$\rho\left(u\frac{\partial u}{\partial r}+w\frac{\partial u}{\partial z}\right)=-\frac{\partial p}{\partial r}+\mu\left\{\frac{\partial}{\partial r}\left[\frac{1}{r}\frac{\partial(ru)}{\partial r}\right]+\frac{\partial^2 u}{\partial z^2}\right\} \quad (1)$$

$$\rho\left(u\frac{\partial w}{\partial r}+w\frac{\partial w}{\partial z}\right)=-\frac{\partial p}{\partial z}+\mu\left\{\frac{\partial}{\partial r}\left[\frac{1}{r}\frac{\partial}{\partial r}\left(r\frac{\partial w}{\partial r}\right)\right]+\frac{\partial^2 w}{\partial z^2}\right\} \quad (2)$$

The equation of continuity is given by:

$$\frac{1}{r}\frac{\partial(ru)}{\partial r}+\frac{\partial w}{\partial z}=0. \quad (3)$$

Due to the axisymmetry of the flow, the following conditions can be applied:

$$u = 0 \quad \text{as} \quad r = 0 \tag{4}$$
$$\frac{\partial w}{\partial r} = 0 \quad \text{as} \quad r = 0 \tag{5}$$

The components of velocity are and w in the radial and axial directions, p is the pressure, μ is the viscosity of the fluid, and ρ is the density. It is assumed that no force acts on the fluid, and, all derivatives $\frac{\partial}{\partial \theta}$ are set to zero, and $u_\theta = 0$.

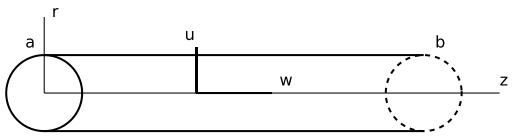

Fig. 1: Sketch of slip flow through a pipe of variable radius

3. Slip condition

This problem is distinct since it relies on slip flow along the wall. The flow geometry may be specified using an orthogonal curvilinear coordinate system to determine the relevant boundary condition. Here n the corresponding distance measured normal to the surface, s measures the distance of a point along the surface, and the corresponding velocity components (u_s, u_n). The slip velocity formula. According to the Newtonian model used to construct the Navier-Stokes relations, it is seen as a linear function of the velocity gradient in the present setting (Vasudeviah et al., 1999). Consequently, the slip velocity generates the correct boundary condition:

$$u_s = -C\ell \frac{\partial u_s}{\partial n}, \quad \text{on} \quad r = R(z) \tag{6}$$

In this context, ℓ is the fluid molecules' mean free path, the slip-coefficient C and let $C = 1.14664$. From condition (6), we observe that $u_s = (u, w).\hat{s}$ and $\frac{\partial u_s}{\partial n} = \nabla u_s.\hat{n}$, then,

$$w + u\frac{dR(z)}{dz} = -C\ell\left[\frac{\partial w}{\partial r} + \frac{\partial u}{\partial r}\frac{dR(z)}{dz} - \frac{1}{2}\frac{\partial w}{\partial r}\left(\frac{dR(z)}{dz}\right)^2 - \frac{\partial w}{\partial z}\frac{dR(z)}{dz} + \ldots\ldots\right], \quad \text{on} \quad r = R(z). \tag{7}$$

Stream function ψ, defined by:

$$w = \frac{1}{r}\frac{\partial \psi}{\partial r}, \quad u = -\frac{1}{r}\frac{\partial \psi}{\partial z}, \tag{8}$$

which must satisfy the boundary conditions (3)

$$\psi = \psi_0 \quad \text{on} \quad r = R(z) \tag{9}$$
$$\psi = O(r^2) \quad \text{as} \quad r \to 0 \tag{10}$$

While conditions (9) and (10) specify the constant flow rat$q$. Conditions (9) and (10) also specify a velocity scale W_0 defined by $W_0 = {}^{q}/_{\pi R_0^2}$, the parameter R_0 being a length scale (e.g. the mean radius of the tube).

Condition (9) also implies the boundary conditions used by Manton (1971), i.e.

$$\frac{1}{r}\frac{\partial \psi}{\partial z} \to 0 \quad \text{as} \quad r \to 0, \quad \frac{\partial}{\partial r}\left(\frac{1}{r}\frac{\partial \psi}{\partial r}\right) \to 0 \quad \text{as} \quad r \to 0. \tag{11}$$

Along the tube's axis, the solution remains regular.

Dimensionless variable: Using the following non-dimension variable:

$$r^* = \frac{r}{R_0}, \quad z^* = \frac{z}{R_0}, \quad \psi^* = \frac{\psi}{\psi_0}, \quad u^* = \frac{2u}{W_0}, \quad w^* = \frac{2w}{W_0},$$
$$Re = \frac{\rho\tau\psi_0}{R_0\mu}, \quad g(z) = \frac{R(z)}{R_0}, \quad Kn = \frac{l}{R_0}, \quad \beta = CKn, \tag{12}$$

where, Re, $g(z)$ and Kn are Low Reynolds number, functional without dimensions for the tube's border and Knudsen number, respectively. See what happens when you use as the stream function's scale factor, differentiate Eq. 1 with respect to and Eq. 2 for, and then subtract the two equations (Van Dyke 1987).

$$D^4\psi = \frac{Re}{r\left(\frac{2}{r}\frac{\partial \psi}{\partial z} + \frac{\partial \psi}{\partial r}\frac{\partial}{\partial z} - \frac{\partial \psi}{\partial z}\frac{\partial}{\partial r}\right)^2} \tag{13}$$

where, $D^2\psi = \frac{\partial^2 \psi}{\partial r^2} - \frac{1}{r}\frac{\partial \psi}{\partial r} + \frac{\partial^2 \psi}{\partial z^2}$.

The boundary conditions become:

$$\left.\begin{aligned} &\psi = 1 \\ &\frac{1}{r}\frac{\partial \psi}{\partial r} + \beta\frac{\partial}{\partial r}\left(\frac{1}{r}\frac{\partial \psi}{\partial r}\right) = \frac{1}{r}\frac{\partial \psi}{\partial z}\frac{dg}{dz} + \\ &\beta\left[\frac{\partial}{\partial r}\left(\frac{1}{r}\frac{\partial \psi}{\partial z}\right)\frac{dg}{dz} + \frac{1}{2}\frac{\partial}{\partial r}\left(\frac{1}{r}\frac{\partial \psi}{\partial r}\right)\left(\frac{dg}{dz}\right)^2 + \frac{1}{r}\frac{\partial^2 \psi}{\partial r \partial z}\frac{dg}{dz}\right] \end{aligned}\right\} \quad \text{on} \quad r = g(z) \tag{14}$$

$$\left.\begin{aligned} &\frac{1}{r}\frac{\partial \psi}{\partial z} \to 0 \\ &\frac{\partial}{\partial r}\left(\frac{1}{r}\frac{\partial \psi}{\partial r}\right) \to 0 \end{aligned}\right\} \quad \text{as } r \to 0 \tag{15}$$

For a small dimensionless perturbation parameter ε (in the limit$\varepsilon \to 0$, the tube is of constant radius), contraction of the axial coordinate to $Z = \varepsilon z$ transform the differential Eq. 13 then,

$$\left(\frac{\partial^2}{\partial r^2} - \frac{1}{r}\frac{\partial}{\partial r} + \varepsilon^2\frac{\partial^2}{\partial z^2}\right)^2 \psi = \frac{\varepsilon Re}{r\left(\frac{2}{r}\frac{\partial \psi}{\partial z} + \frac{\partial \psi}{\partial r}\frac{\partial}{\partial r} - \frac{\partial \psi}{\partial z}\frac{\partial}{\partial r}\right)\left(\frac{\partial^2 \psi}{\partial r^2} - \frac{1}{r}\frac{\partial \psi}{\partial r} + \varepsilon^2\frac{\partial^2 \psi}{\partial z^2}\right)} \tag{16}$$

4. Perturbation solution

To overcome the current issue, we increase the flow quantities in a power series with a tiny parameter ε as follows:

$$u = u_0 + \varepsilon u_1 + \varepsilon^2 u_2 + O(\varepsilon^3)$$
$$w = w_0 + \varepsilon w_1 + \varepsilon^2 w_2 + O(\varepsilon^3)$$
$$\psi = \psi_0 + \varepsilon \psi_1 + \varepsilon^2 \psi_2 + O(\varepsilon^3). \tag{17}$$

Substituting Eq. 17 in Eqs. 14, 15, and 16 while amassing coefficients with similar powers ofε, one gets the zero-order equation as:

$$\left(\frac{\partial^2}{\partial r^2}-\frac{1}{r}\frac{\partial}{\partial r}\right)^2\psi_0=0 \tag{18}$$

and

$$\left.\begin{array}{l}\psi_0=1\\ \frac{1}{r}\frac{\partial\psi_0}{\partial r}+\beta\frac{\partial}{\partial r}\left(\frac{1}{r}\frac{\partial\psi_0}{\partial r}\right)=0\end{array}\right\}$$

on the wall of the pipe

$$\left.\begin{array}{l}\mathrm{r}=\mathrm{h(Z)}\\ \frac{1}{r}\frac{\partial\psi_0}{\partial Z}\to 0\\ \frac{\partial}{\partial r}\left(\frac{1}{r}\frac{\partial\psi_0}{\partial r}\right)\to 0\end{array}\right\} \quad \text{as} \quad r\to 0 \tag{19, 20}$$

where,

$$\mathrm{g(z)=h(Z).} \tag{21}$$

The solution of the set Eqs. 18-21 give the stream function components as:

$$\psi_0=\frac{1}{4\beta+\mathrm{h}}[2(2\beta+\mathrm{h})\eta^2-\mathrm{h}\eta^4] \tag{22}$$

where, $\eta=\frac{\mathrm{r}}{\mathrm{h}}$

In view of Eq. 16, the ε-order equation is:

$$\left(\frac{\partial^2}{\partial r^2}-\frac{1}{r}\frac{\partial}{\partial r}\right)^2\psi_1=\frac{Re}{r\left(\frac{2\partial\psi_0}{r\,\partial Z}+\frac{\partial\psi_0}{\partial r}\frac{\partial}{\partial Z}-\frac{\partial\psi_0}{\partial Z}\frac{\partial}{\partial r}\right)\left(\frac{\partial^2\psi_0}{\partial r^2}-\frac{1}{r}\frac{\partial\psi_0}{\partial r}\right)} \tag{23}$$

Moreover,

$$\left.\begin{array}{l}\psi_1=0\\ \frac{1}{r}\frac{\partial\psi_1}{\partial r}+\beta\frac{\partial}{\partial r}\left(\frac{1}{r}\frac{\partial\psi_1}{\partial r}\right)=0\end{array}\right\},$$

on the wall of the pipe

$$\left.\begin{array}{l}\mathrm{r}=\mathrm{h(Z)}\\ \frac{1}{r}\frac{\partial\psi_1}{\partial Z}\to 0\\ \frac{\partial}{\partial r}\left(\frac{1}{r}\frac{\partial\psi_1}{\partial r}\right)\to 0\end{array}\right\} \quad \text{as} \quad r\to 0 \tag{24, 25}$$

Solving Eqs. 23-25, one obtains:

$$\psi_1=\frac{\mathrm{h'\,Re}(3\beta+\mathrm{h})}{9(2\beta+\mathrm{h})(4\beta+\mathrm{h})^3}\{4(2\beta+\mathrm{h})(6\beta+\mathrm{h})\eta^2-[2\mathrm{h}(6\beta+\mathrm{h})+(72\beta^2+42\beta\mathrm{h}+7\mathrm{h}^2)]\eta^4+6(2\beta+\mathrm{h})^2\eta^6-\mathrm{h}(2\beta+\mathrm{h})\eta^8\}. \tag{26}$$

The ε^2-order equation is:

$$\left(\frac{\partial^2}{\partial r^2}-\frac{1}{r}\frac{\partial}{\partial r}\right)^2\psi_2+\left(\frac{\partial^2}{\partial r^2}-\frac{1}{r}\frac{\partial}{\partial r}\right)\frac{\partial^2\psi_0}{\partial Z^2}+\frac{\partial^2}{\partial Z^2}\left(\frac{\partial^2\psi_0}{\partial r^2}-\frac{1}{r}\frac{\partial\psi_0}{\partial r}\right)==\frac{Re}{r\left[\left(\frac{2\partial\psi_0}{r\,\partial Z}+\frac{\partial\psi_0}{\partial r}\frac{\partial}{\partial Z}-\frac{\partial\psi_0}{\partial Z}\frac{\partial}{\partial r}\right)\left(\frac{\partial^2\psi_1}{\partial r^2}-\frac{1}{r}\frac{\partial\psi_1}{\partial r}\right)\right.}+\left(\frac{2}{r}\frac{\partial\psi_1}{\partial Z}+\frac{\partial\psi_1}{\partial r}\frac{\partial}{\partial Z}-\left.\frac{\partial\psi_1}{\partial Z}\frac{\partial}{\partial r}\right)\left(\frac{\partial^2\psi_0}{\partial r^2}-\frac{1}{r}\frac{\partial\psi_0}{\partial r}\right)\right] \tag{27}$$

In addition, the corresponding boundary conditions are:

$$\left.\begin{array}{l}\psi_2=0\\ \frac{1}{\mathrm{r}}\frac{\partial\psi_2}{\partial \mathrm{r}}+\beta\frac{\partial}{\partial \mathrm{r}}\left(\frac{1}{\mathrm{r}}\frac{\partial\psi_2}{\partial \mathrm{r}}\right)=\mathrm{f(r,z)}\end{array}\right\}\ \text{on r = h(Z)} \tag{28}$$

$$\left.\begin{array}{l}\frac{1}{\mathrm{r}}\frac{\partial\psi_2}{\partial \mathrm{Z}}\to 0\\ \frac{\partial}{\partial \mathrm{r}}\left(\frac{1}{\mathrm{r}}\frac{\partial\psi_2}{\partial \mathrm{r}}\right)\to 0\end{array}\right\}\ \text{as r}\to 0 \tag{29}$$

where,

$$\mathrm{f(r,z)}=\frac{1}{\mathrm{r}}\frac{\partial\psi_0}{\partial \mathrm{z}}\frac{\mathrm{dh}}{\mathrm{dz}}+\beta\left[\frac{\partial}{\partial \mathrm{r}}\left(\frac{1}{\mathrm{r}}\frac{\partial\psi_0}{\partial \mathrm{z}}\right)\frac{\mathrm{dh}}{\mathrm{dz}}+\frac{1}{2}\frac{\partial}{\partial \mathrm{r}}\left(\frac{1}{\mathrm{r}}\frac{\partial\psi_0}{\partial \mathrm{r}}\right)\left(\frac{\mathrm{dh}}{\mathrm{dz}}\right)^2+\frac{1}{\mathrm{r}}\frac{\partial^2\psi_0}{\partial \mathrm{r}\,\partial \mathrm{z}}\frac{\mathrm{dh}}{\mathrm{dz}}\right].$$

Solving Eqs. 27-29 on obtains:

$$\psi_2=\frac{1}{3(4\beta+\mathrm{h})^4}(12\beta(4\beta+\mathrm{h})(1+\mathrm{h})(\eta^2-\eta^4)\mathrm{hh'}+(\delta_1\eta^2-2\delta_2\eta^4+\delta_3\eta^6)\mathrm{h'^2}-(4\beta+\mathrm{h})(3\beta+\mathrm{h})[(8\beta+\mathrm{h})\eta^2-2(6\beta+\mathrm{h})\eta^4+(4\beta+\mathrm{h})\eta^6]\mathrm{h^2h''})+\frac{\mathrm{Re}^2}{2700(4\beta+\mathrm{h})^6}\left[\frac{\mathrm{h'^2}}{\mathrm{h}}(2\lambda_1\eta^2-5\lambda_2\eta^4+50\lambda_3\eta^6-75\lambda_4\eta^8+30\lambda_5\eta^{10}-2\lambda_6\mu^{12})-3(3\beta+\mathrm{h})(4\beta+\mathrm{h})\mathrm{h''}(4\alpha_1\eta^2-5\alpha_2\eta^4+150\alpha_3\eta^6-25\alpha_4\eta^8+20\alpha_5\eta^{10}-2\alpha_6\eta^{12})\right] \tag{30}$$

where,

$$\left.\begin{array}{l}\delta_1=384\beta^4+624\beta^3\mathrm{h}+324\beta^2\mathrm{h}^2+70\beta\mathrm{h}^3+5\mathrm{h}^4\\ \delta_2=192\beta^4+408\beta^3\mathrm{h}+246\beta^2\mathrm{h}^2+60\beta\mathrm{h}^3+5\mathrm{h}^4\\ \delta_3=\mathrm{h}(4\beta+\mathrm{h})(48\beta^2+30\beta\mathrm{h}+5\mathrm{h}^4)\end{array}\right\}.$$

The h′and h′′are the first and the second derivatives of h with respect to Z and

$$\left.\begin{array}{l}\lambda_1=403200\beta^5+510480\beta^4\mathrm{h}+258000\beta^3\mathrm{h}^2+65001\beta^2\mathrm{h}^3+8180\beta\mathrm{h}^4+409\mathrm{h}^5\\ \lambda_2=276480\beta^5+388800\beta^4\mathrm{h}+218928\beta^3\mathrm{h}^2+61548\beta^2\mathrm{h}^3+8622\beta\mathrm{h}^4+479\mathrm{h}^5\\ \lambda_3=(4\beta+\mathrm{h})(3456\beta^4+5184\beta^3\mathrm{h}+2772\beta^2\mathrm{h}^2+636\beta\mathrm{h}^3+43\mathrm{h}^4)\\ \lambda_4=(4\beta+\mathrm{h})(384\beta^4+960\beta^3\mathrm{h}+676\beta^2\mathrm{h}^2+190\beta\mathrm{h}^3+19\mathrm{h}^4)\\ \lambda_5=\mathrm{h}(4\beta+\mathrm{h})(252\beta^3+281\beta^2\mathrm{h}+104\beta\mathrm{h}^2+13\mathrm{h}^3)\\ \lambda_6=\mathrm{h}^2(4\beta+\mathrm{h})(180\beta^2+114\beta\mathrm{h}+19\mathrm{h}^2)\end{array}\right\} \tag{31}$$

and

$$\left\{\begin{array}{l}\alpha_1 = 1400\beta^3 + 860\beta^2 h + 182\beta h^2 + 13h^3\\ \alpha_2 = 1920\beta^3 + 1400\beta^2 h + 348\beta h^2 + 29h^3\\ \alpha_3 = (4\beta + h)^2(2\beta + h)\\ \alpha_4 = (4\beta + h)(8\beta^2 + 12\beta h + 3h^2)\\ \alpha_5 = h(4\beta + h)(2\beta + h)\\ \alpha_6 = h^2(4\beta + h)\end{array}\right\} \quad (32)$$

5. Axial and radial velocities

Using Eq. 7 and Eqs. 22, 26, and 30, the axial velocity w, non-dimensionalized by R_0 and ψ_0 can be expressed as:

$$w = \frac{4}{h^2(4\beta+h)}(2\beta + h - h\eta^2) + \frac{4(3\beta+h)h'Re\epsilon}{9h^2(2\beta+h)(4\beta+h)^3}[2(2\beta + h)(6\beta + h) - [2h(6\beta + h) + (72\beta^2 + 42\beta h + 7h^2)]\eta^2 + 9(2\beta + h)^2\eta^4 - 2h(2\beta + h)\eta^6] + \frac{2\epsilon^2}{3h^2(4\beta+h)^4}\left(4\beta(1 + h)(4\beta + h)(1 - 6(4\beta + h)\eta^2)hh' + (\delta_1 - 4\delta_2\eta^2 + 3\delta_3\eta^4)h'^2 - (3\beta + h)(4\beta + h)[(8\beta + h) - 4(6\beta + h)\eta^2 + 3(4\beta + h)\eta^4]h^2h''\right) + \frac{Re^2\epsilon^2}{2700h^2(4\beta+h)^6}[\frac{4h'^2}{h}(\lambda_1 - 5\lambda_2\eta^2 + 75\lambda_3\eta^4 - 150\lambda_4\eta^6 + 75\lambda_5\eta^8 - 6\lambda_6\eta^{10}) - 12(3\beta + h)(4\beta + h)h''(2\alpha_1 - 5\alpha_2\eta^2 + 225\alpha_3\eta^4 - 50\alpha_4\eta^6 + 50\alpha_5\eta^8 - 6\alpha_6\eta^{10})] + O(\epsilon^2). \quad (33)$$

In addition, the radial velocity u, nondimensionalized by R_0 and ψ_0, expressed as:

$$u = \frac{4h'}{h^2(4\beta+h)^2}[(8\beta^2 + 5\beta h + h^2)\eta - h(3\beta + h)\eta^3] + \frac{Re\epsilon}{9(4\beta+h)^4}\left\{\frac{h'^2}{h^2}[12(48\beta^3 + 42\beta^2 h + 12\beta h^2 + h^3)\eta - 9(4\beta + h)(48\beta^2 + 30\beta h + 5h^2)\eta^3 + 6(144\beta^3 + 154\beta^2 h + 56\beta h^2 + 7h^3)\eta^5 - 3h(28\beta^2 + 18\beta h + 3h^2)\eta^7] - (3\beta + h)(4\beta + h)\frac{h''}{h}[4(6\beta + h)\eta - 9(4\beta + h)\eta^3 + 6(2\beta + h)\eta^5 - h\eta^7]\right\} + \epsilon^2\left\{\frac{4\beta h'^2}{h(4\beta+h)^3}[(4\beta + 3h + 2h^2)\eta - (12\beta + 5h + 5\beta h + 4h^2)\eta^3] - \frac{4\beta(1+h)h''}{(4\beta+h)^2}(\eta - \eta^3) + \frac{2h'^3}{3h^2(4\beta+h)^5}[c_1\eta - 4c_2\eta^3 + 3c_3\eta^5] - \frac{h'h''}{2h(4\beta+h)^4}[c_4\eta - 2c_5\eta^3 + 3\delta_3\eta^5] + \frac{h(3\beta+h)h'''}{3(4\beta+h)^3}[(8\beta + h)\eta - 2(6\beta + h)\eta^3 + (4\beta + h)\eta^5] + \frac{h'^3Re^2}{1350h^3(4\beta+h)^7}[2a_1\eta - 15a_2\eta^3 + 200a_3\eta^5 - 75a_4\eta^7 + 30a_5\eta^9 - 2a_6\eta^{11}] + \frac{(3\beta+h)Re^2h'''}{900h(4\beta+h)^5}[4\alpha_1\eta - 5\alpha_2\eta^3 + 150\alpha_3\eta^5 - 25\alpha_4\eta^7 + 20\alpha_5\eta^9 - 2\alpha_6\eta^{11}] - \frac{Re^2h'h''}{2700h^2(4\beta+h)^6}[4b_1\eta - 5b_2\eta^3 + 50b_3\eta^5 - 75b_4\eta^7 + 180b_5\eta^9 - 2b_6\eta^{11}]\right\} + O(\epsilon^3) \quad (34)$$

where,

$$\begin{aligned}c_1 &= 1536\beta^5 + 2400\beta^4 h + 1560\beta^3 h^2 + 508\beta^2 h^3 + 85\beta h^4 + 5h^5\\ c_2 &= 768\beta^5 + 1608\beta^4 h + 1206\beta^3 h^2 + 429\beta^2 h^3 + 75\beta h^4 + 5h^5\\ c_3 &= (4\beta + h)(160\beta^3 + 144\beta^2 h + 45\beta h^2 + 5h^3)\\ c_4 &= 768\beta^4 + 1248\beta^3 h + 676\beta^2 h^2 + 154\beta h^3 + 11h^4\\ c_5 &= 384\beta^4 + 960\beta^3 h + 618\beta^2 h^2 + 156\beta h^3 + 13h^4,\end{aligned} \quad (35)$$

$$\begin{aligned}a_1 &= 2419200\beta^6 + 3856320\beta^5 h + 255792\beta^4 h^2 + 903000\beta^3 h^3 + 178643\beta^2 h^4 + 18814\beta h^5 + 818h^6\\ a_2 &= 921600\beta^6 + 1543680\beta^5 h + 1085856\beta^4 h^2 + 410456\beta^3 h^3 + 87812\beta^2 h^4 + 10059\beta h^5 + 479h^6\\ a_3 &= (4\beta + h)(12096\beta^5 + 20736\beta^4 h + 14058\beta^3 h^2 + 4737\beta^2 h^3 + 795\beta h^4 + 53h^5)\\ a_4 &= (4\beta + h)(6912\beta^5 + 18048\beta^4 h + 15704\beta^3 h^2 + 6336\beta^2 h^3 + 1235\beta h^4 + 95h^5)\\ a_5 &= h(4\beta + h)(5040\beta^4 + 6948\beta^3 h + 3631\beta^2 h^2 + 858\beta h^3 + 78h^4)\\ a_6 &= h^2(4\beta + h)(3960\beta^3 + 3720\beta^2 h + 1197\beta h^2 + 133h^3)\end{aligned} \quad (36)$$

and

$$\begin{aligned}b_1 &= 504000\beta^5 + 646440\beta^4 h + 329640\beta^3 h^2 + 83439\beta^2 h^3 + 10520\beta h^4 + 526h^5\\ b_2 &= 82944\beta^5 + 1153440\beta^4 h + 643392\beta^3 h^2 + 179640\beta^2 h^3 + 25074\beta h^4 + 1393h^5\\ b_3 &= (4\beta + h)(12096\beta^4 + 17208\beta^3 h + 8946\beta^2 h^2 + 2028\beta h^3 + 169h^4)\\ b_4 &= (4\beta + h)(1536\beta^4 + 3440\beta^3 h + 2340\beta^2 h^2 + 650\beta h^3 + 65h^4)\\ b_5 &= h(4\beta + h)(156\beta^3 + 173\beta^2 h + 64\beta h^2 + 8h^3)\\ b_6 &= h^2(4\beta + h)(720\beta^2 + 462\beta h + 77h^2).\end{aligned} \quad (37)$$

For ($Re \to 0$), the terms containing Re omitted, and the axial and radial velocities simplified as:

$$w = \frac{4}{h^2(4\beta+h)}(2\beta + h - h\eta^2) + \frac{2\epsilon^2}{3h^2(4\beta+h)^4}\left(4\beta(1 + h)(4\beta + h)(1 - 6(4\beta + h)\eta^2)hh' + (\delta_1 - 4\delta_2\eta^2 + 3\delta_3\eta^4)h'^2 - (3\beta + h)(4\beta + h)[(8\beta + h) - 4(6\beta + h)\eta^2 + 3(4\beta + h)\eta^4]h^2h''\right) + O(\epsilon^2) \quad (38)$$

$$u = \frac{4h'}{h^2(4\beta+h)^2}[(8\beta^2 + 5\beta h + h^2)\eta - h(3\beta + h)\eta^3] + \epsilon^2\left\{\frac{4\beta h'^2}{h(4\beta+h)^3}[(4\beta + 3h + 2h^2)\eta - (12\beta + 5h + 5\beta h + 4h^2)\eta^3] - \frac{4\beta(1+h)h''}{(4\beta+h)^2}(\eta - \eta^3) + \frac{2h'^3}{3h^2(4\beta+h)^5}[c_1\eta - 4c_2\eta^3 + 3c_3\eta^5] - \frac{h'h''}{2h(4\beta+h)^4}[c_4\eta - 2c_5\eta^3 + 3\delta_3\eta^5] + \frac{h(3\beta+h)h'''}{3(4\beta+h)^3}[(8\beta + h)\eta - 2(6\beta + h)\eta^3 + (4\beta + h)\eta^5]\right\} + O(\epsilon^3) \quad (39)$$

6. Discussion

Here, when $\beta \to 0$, the solution of the stream function (22), (26) and (30) coincide well with Van Dyke (1987) and Sisavath et al. (2001b). The solutions of the axial and radial velocities (38) and (39) coincide with Kotorynski (1995). Following Sisavath et al. (2001b), the length scale R_0 as the

mean radius of the constricted tube, and dimensionless length scale $\tilde{\lambda}$ defined as $\tilde{\lambda} = {}^{\lambda}/_{R_0}$, where λ is the wavelength of the constriction. The Reynolds number is calculated using Eq. 11 and can easily be connected to other definitions used if necessary. Let R(z) as:

$$R(z) = R_0\left[1 + \frac{\delta}{R_0}\sin\left(\frac{2\pi z}{\lambda}\right)\right], \quad (40)$$

where, z is the axial distance from the throat of the constriction (i.e. from the point of minimum radius). In accordance with the requirement that the tube profile be slowly varying, an appropriate small perturbation parameter is

$$\epsilon = {}^{\tilde{\delta}}/_{\tilde{\lambda}}, \quad (41)$$

where, $\delta = {}^{\tilde{\delta}}/_{R_0}$ is the dimensionless amplitude of the constriction, $x = r/R$.

For different constriction configurations, the axial velocity profiles obtained from Eq. 38 are shown in Figs. 2-5, while the radial velocity profiles obtained from Eq. 39 are displayed in Figs. 6 and 7 for the same configurations.

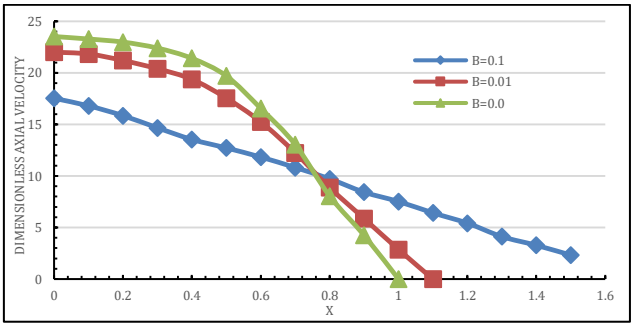

Fig. 2: Axial velocity profiles at the throat $\frac{z}{\lambda} = -0.25$ for the geometry $\tilde{\delta} = 0.6, \tilde{\lambda} = 5$

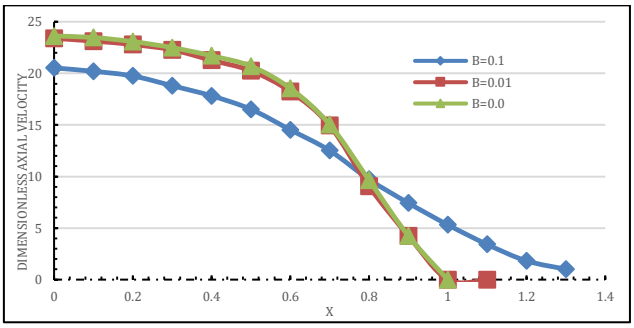

Fig. 3: Axial velocity profiles at the top of the expansion region $\frac{z}{\lambda} = 0.25$ for the geometry $\tilde{\delta} = 0.6, \tilde{\lambda} = 5$

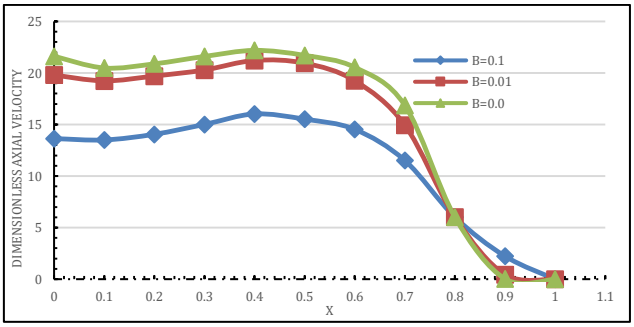

Fig. 4: Axial velocity patterns at the throat $\frac{z}{\lambda} = -0.25$ for the geometry $\tilde{\delta} = 0.3, \tilde{\lambda} = 2$

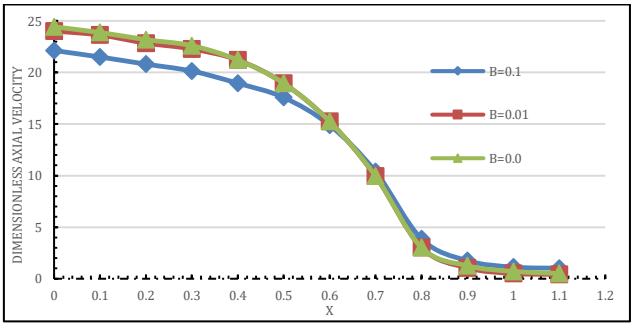

Fig. 5: Profiles of axial velocities at the expansion region's peak $\frac{z}{\lambda} = 0.25$ for the geometry $\tilde{\delta} = 0.3, \tilde{\lambda} = 2$

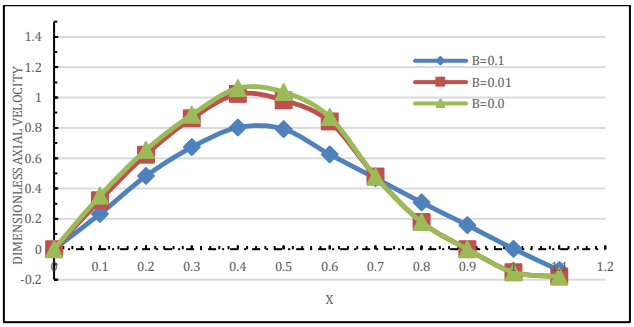

Fig. 6: Radial velocity profiles at the location $\frac{z}{\lambda} = 0$ for the geometry$\tilde{\delta} = 0.6, \tilde{\lambda} = 5$

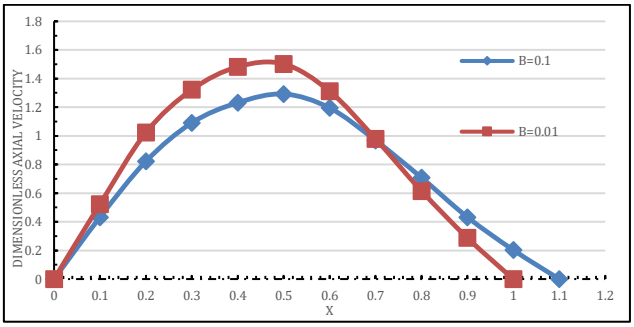

Fig. 7: Radial velocity profiles at the location $\frac{z}{\lambda} = 0$ for the geometry $\tilde{\delta} = 0.3, \tilde{\lambda} = 2$

7. Conclusion

Here, it may be noted that, as a no-slip condition ($\beta \to 0$), the axial velocity profile calculated using Eq. 38 which is displayed in Figs. 2-5 at various cross-sections of the tube (the throat $\frac{z}{\lambda} = -0.25$ and the top of the expansion $\frac{z}{\lambda} = 0.25$), and for various geometry $\tilde{\delta}$ and $\tilde{\lambda}$, coincides well with results. As the slip condition, the axial velocity profile increases with the increase in the slip coefficient,β, at the wall of the tube and decreases at the center of the tube ($r = 0$). The radial velocity profile obtained for this configuration using Eq. 39 is also displayed in Figs. 5-6 in the region ($\frac{z}{\lambda} = 0$). Our research shows that radial velocities are much greater close to the centerline and have negative values close to the tube wall because of flow reversal. Also, as the slip coefficient goes up, the radial velocity profile goes up too. Typically, when the wall temperature and wall heat flux are both constant, the converse is true for velocity slip and temperature leap: under these circumstances, a large slip on the wall enhances convection down the surface, whereas temperature leap has the opposite effect. The opposite is true for large temperature jumps; they decrease heat transmission by reducing the wall temperature gradient. Consequently, the heat transfer coefficient will be overestimated if the temperature increase is ignored. After that, the thermal conductivity and temperature-variable dynamic viscosity of the fluid were measured and compared to microchannel constant property findings taking rarefaction and viscous dissipation into account. Here is a summary of the findings about microscale slip flow:

- It is important to include property variation effects in numerical solutions of microchannel airflow when the entrance length is like the channel length. Nevertheless, the constant property assumption will provide adequate findings for long channels with entry lengths that are negligible relative to the total channel length.
- When thermophysical properties alter, it affects the temperature profile. Fluid heating and cooling experience substantial local number fluctuations in the growing area because of temperature-changing properties.

List of symbols

r	Radial coordinate
z	Axial coordinate
R(z)	Radius of the tube as a function of z
u	Axial velocity component
v	Radial velocity component
p	Pressure
μ	Dynamic viscosity
ρ	Fluid density
λ	Fluid molecule mean free path
φ	Stream function
ψ	Perturbation stream function component
ε	Small perturbation parameter
η	Dimensionless radial coordinate
ζ	Dimensionless axial coordinate
α	Length scale
β	Slip coefficient
Re	Reynolds number
Kn	Knudsen number
δ	Dimensionless wavelength parameter
A_0, A_1, A_2	Coefficients/functions in the stream function expansions
∂	Partial derivative symbol

Acknowledgment

The authors gratefully acknowledge the approval and support of this research study by Grant No. NBU-

FFR-2024-1695-03 from the Deanship of Scientific Research in Northern Border University, Arar, KSA.

Compliance with ethical standards

Conflict of interest

The author(s) declared no potential conflicts of interest with respect to the research, authorship, and/or publication of this article.

References

Bilal M, Siddique I, Borawski A, Raza A, Nadeem M, and Sallah M (2022). Williamson magneto nanofluid flow over partially slip and convective cylinder with thermal radiation and variable conductivity. Scientific Reports, 12(1): 12727. https://doi.org/10.1038/s41598-022-16268-2 **PMid:35882915 PMCid:PMC9325731**

Boraey MA and Guaily A (2021). Analytical solution for the quasi-two dimensional non-isothermal fully developed flow of molten salt in a circular pipe. Physics of Fluids, 33(11): 113601. https://doi.org/10.1063/5.0065313

Chakravarty SI and Sen S (2008). Analysis of pulsatile blood flow in constricted bifurcated arteries with vorticity-stream function approach. Journal of Medical Engineering and Technology, 32(1): 10-22. https://doi.org/10.1080/03091900600700822 **PMid:18183516**

Chow JC and Soda K (1972). Laminar flow in tubes with constriction. The Physics of Fluids, 15(10): 1700-1706. https://doi.org/10.1063/1.1693765

Chu Z (2000). Slip flow in an annulus with corrugated walls. Journal of Physics D: Applied Physics, 33(6): 627-631. https://doi.org/10.1088/0022-3727/33/6/307

El-Khatib FH and Damiano ER (2003). Linear and nonlinear analyses of pulsatile blood flow in a cylindrical tube. Biorheology, 40(5): 503-522. https://doi.org/10.1177/0006355X2003040005003

Elshahed M (2004). Blood flow in capillary under starling hypothesis. Applied Mathematics and Computation, 149(2): 431-439. https://doi.org/10.1016/S0096-3003(03)00151-6

Fusi L, Housiadas KD, and Georgiou GC (2020). Flow of a Bingham fluid in a pipe of variable radius. Journal of Non-Newtonian Fluid, 285: 104393. https://doi.org/10.1016/j.jnnfm.2020.104393

Hemmat M and Borhan A (1995). Creeping flow through siunoidally constricted capillaries. Physics of Fluids, 7(9): 2111-2121. https://doi.org/10.1063/1.868462

Kakaç S, Yazıcıoğlu AG, and Gözükara AC (2011). Effect of variable thermal conductivity and viscosity on single-phase convective heat transfer in slip flow. Heat Mass Transfer, 47(8): 879–891. https://doi.org/10.1007/s00231-011-0851-3

Khalafvand SS and Han HC (2015). Stability of carotid artery under steady state and pulsatile blood flow: A fluid-structure interaction study. Journal of Biomechanical Engineering, 137(6): 061007. https://doi.org/10.1115/1.4030011 **PMid:25761257 PMCid:PMC5101041**

Koplik J (1982). Creeping flow in tow-dimensional networks. Journal Fluid Mechanics, 119: 219-247. https://doi.org/10.1017/S0022112082001323

Kotorynski WP (1995). Viscous flow in axisymmetric pipes with slow variations. Computer and Fluids, 24(6): 685-717. https://doi.org/10.1016/0045-7930(95)00002-T

Manton MJ (1971). Low Reynolds number flow in slowly varying axisymmetric tube. Journal of Fluid Mechanics, 49(3): 451-459. https://doi.org/10.1017/S0022112071002192

Matthews MT and Hill JM (2007). Nano boundary layer equation with nonlinear Navier boundary condition. Journal of Mathematical Analysis and Applications, 333(1): 381–400. https://doi.org/10.1016/j.jmaa.2006.08.047

Matthews MT and Hill JM (2008). A note on the boundary layer equations with linear slip boundary condition. Applied Mathematics Letters, 21(8): 810–813. https://doi.org/10.1016/j.aml.2007.09.002

Pérez-Salas KY, Ascanio G, Ruiz-Huerta L, and Aguayo JP (2021). Approximate analytical solution for the flow of a Phan-Thien–Tanner fluid through an axisymmetric hyperbolic contraction with slip boundary condition. Physics of Fluids, 33(5): 053110. https://doi.org/10.1063/5.0048625

Ponalagusamy RI and Priyadharshini S (2017). Nonlinear model on pulsatile flow of blood through a porous bifurcated arterial stenosis in the presence of magnetic field and periodic body acceleration. Computer Methods and Programs in Biomedicine, 142: 31-41. https://doi.org/10.1016/j.cmpb.2017.02.014 **PMid:28325445**

Rao AR and Devanathan R (1973). Pulsatile flow in tubes of slowly varying cross-section. Journal of Applied Mathematics and Physics (ZAMP), 24: 203-213. https://doi.org/10.1007/BF01590913

Rao IJ and Rajagopal T (1999). The effect of the slip boundary condition on the flow of fluids in channel. Acta Mechanica, 135(3): 113-126. https://doi.org/10.1007/BF01305747

Shankar BM, Jai Kumar, Shivakumara IS, and Naveen Kumar SB (2019). MHD instability of pressure-driven flow of a non-Newtonian fluid. SN Applied Sciences, 1(12): 1523. https://doi.org/10.1007/s42452-019-1557-2

Singh KD (2013). Effect of slip condition on viscoelastic MHD oscillatory forced convection flow in a vertical channel with heat radiation. International Journal of Applied Mechanics and Engineering, 18(4): 1237-1248. https://doi.org/10.2478/ijame-2013-0075

Singh R and Laurence RL (1979). Influence of slip velocity at membrance surface on ultrafiltration performance creeping flow in tow-dimensional networks. International Journal of Heat and Mass Transfer, 22(5): 721-729. https://doi.org/10.1016/0017-9310(79)90119-4

Sisavath S, Jing X, and Zimmerman RW (2001a). Laminar flow through irregularly shaped pores in sedimentary rocks. Transport in Porous Media, 45(1): 41-62. https://doi.org/10.1023/A:1011898612442

Sisavath S, Jing X, and Zimmerman RW (2001b). Creeping flow through a pipe of varying radius. Physics Fluids, 13(10): 2762–2772. https://doi.org/10.1063/1.1399289

Srinivasacharya D and Rao GM (2016). Computational analysis of magnetic effects on pulsatile flow of couple stress fluid through a bifurcated artery. Computer Methods and Programs in Bio-medicine, 137: 269-279. https://doi.org/10.1016/j.cmpb.2016.09.015 **PMid:28110731**

Teimouri K, Tavakoli MR, Ghafari A, and Kim KC (2021). Investigation of the plaque morphology effect on changes of pulsatile blood flow in a stenosed curved artery induced by an external magnetic field. Computers Biology and Medicine, 135: 104600. https://doi.org/10.1016/j.compbiomed.2021.104600 **PMid:34214938**

Terrill RM (1984). A note on laminar flows through a porous pipe with slip. IMA Journal of Applied Mathematics, 33(2): 169-174. https://doi.org/10.1093/imamat/33.2.169

Terrill RM and Thomas PW (1969). On laminar flow through a uniformly porous pipe. Applied Scientific Research, 21: 37–67. https://doi.org/10.1007/BF00411596

Tilton JN and Payatakes AC (1984). Collocation solution of creeping Newtonian through sinusoidal tubes: A correction. AI ChE Journal, 30(6): 1016-1021. https://doi.org/10.1002/aic.690300628

Van Dyke M (1987). Slow variations in continuum mechanics. Advances in Applied Mechanics, 25: 1-45. https://doi.org/10.1016/S0065-2156(08)70276-X

Vasudeviah M and Balaurugan K (1999). Stokes slip flow in a corrugated pipe. International Journal of Engineering, 37(12): 1629-1641. https://doi.org/10.1016/S0020-7225(98)00138-4

White FM (1962). Laminar flow in a uniformly porous pipe. Journal of Applied Mechanics, 29(1): 201–204. https://doi.org/10.1115/1.3636459

Wong CY (2002). Low Reynolds number slip flow in a curved rectangular duct. Journal of Applied Mechanics, 69(2): 189-194. https://doi.org/10.1115/1.1445142